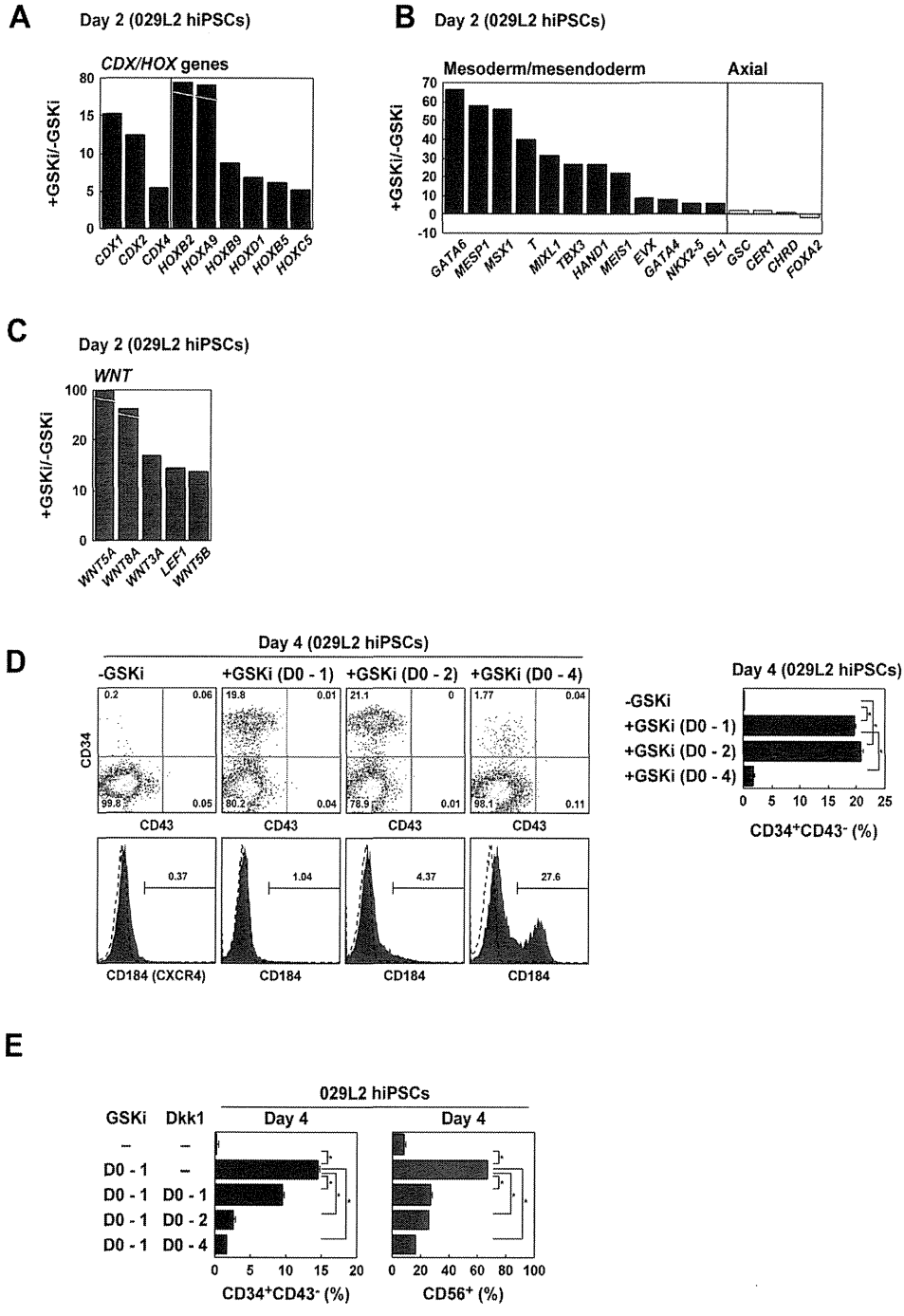

Figure 2. Effects of GSKi treatment on gene expression and HEP induction. (**A**) Upregulation of *CDX/HOX* genes in the GSKi-treated hiPSCs. (**B**) Expression of mesoderm/mesendoderm markers and axial mesoderm markers in the GSKi-treated hiPSCs. (**C**) Expression levels of *WNT*-related genes in the GSKi-treated hiPSCs. (**A–C**) The 029L2 hiPSCs were treated with GSKi (days 0–1) or without GSKi followed by BMP4 treatment. On day 2, RNA was collected and subjected to microarray analysis. Fold changes in relative expression level (+GSKi/−GSKi) are given. (**D**) Induction of $CD34^{+}CD43^{-}$ HEPs by transient GSKi treatment. The 029L2 hiPSCs were differentiated in STEMDiff APEL with or without GSKi, as indicated. On days 1 and 2, BMP4 and VEGF were added, as illustrated in Figure 1A. On day 4, expression of CD34, CD43, and CD184 was analyzed by FACS. (**E**) Effects of WNT inhibitor Dkk1 on GSKi-induced HEP differentiation and EMT. The 029L2 hiPSCs were differentiated in STEMDiff APEL with or without GSKi (days 0–1), followed by 3 days of culture with BMP4 and VEGF, as illustrated in Figure 1A. Dkk1 was added as indicated. On day 4, expression of CD34, CD43, and CD56 was analyzed by FACS. In (**D** and **E**), average percentages ($n = 3$) ± SD are given ($^{*}p < 0.005$).

by GSKi treatment (Fig. 2C). Given the finding that *Wnt* family genes are expressed in the posterior region of embryos [17], it is possible that early GSKi treatment induced the formation of posterior mesoderm cells from hiPSCs via the *LEF1–CDX* axis. Once the hiPSCs acquired posterior mesoderm cell identity, *WNT* expression was initiated; thus, canonical WNT/β-CATENIN signaling could be activated, even in the absence of a GSKi.

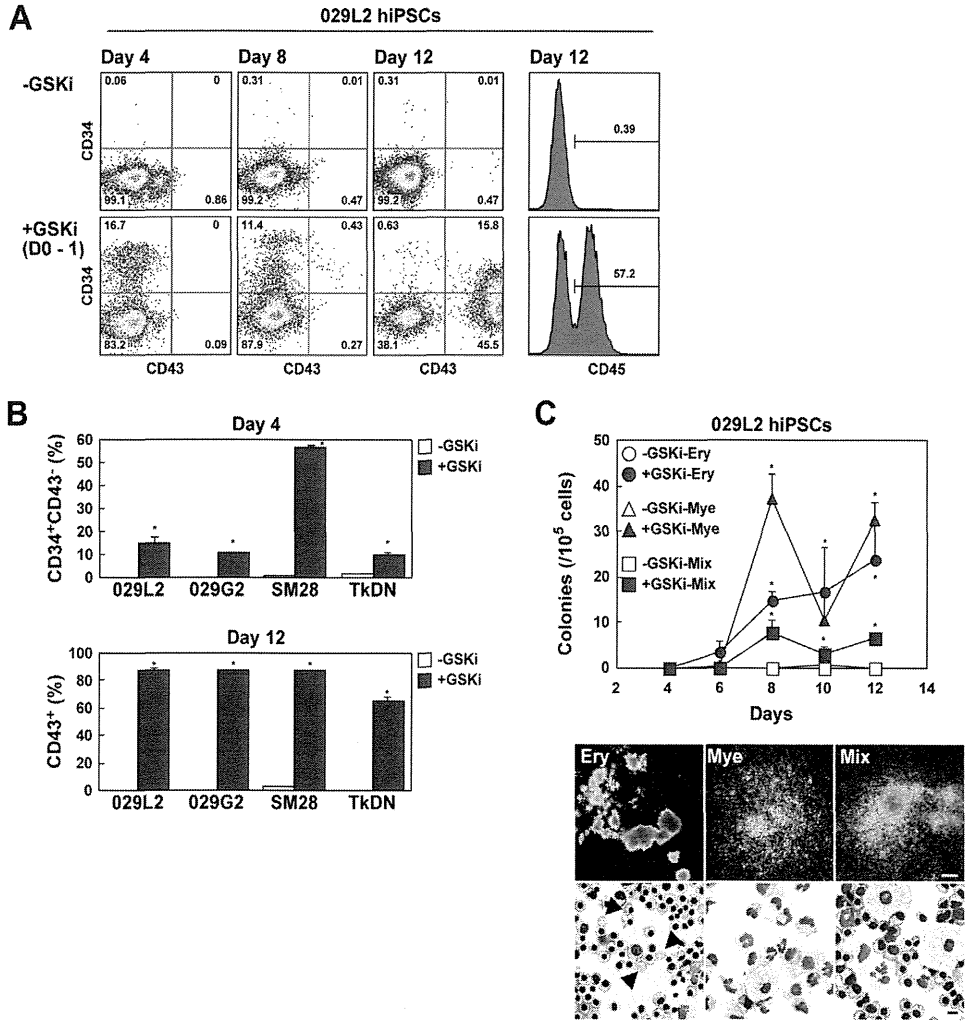

Figure 3. Effects of GSKi treatment on hematopoietic cell differentiation of hiPSCs. (**A**) Effect of GSKi on hematopoietic cell differentiation of 029L2 hiPSCs. On day 4, growth factor cocktails were added, and analyses were conducted on days 8 and 12. (**B**) Percentages of $CD34^+CD43^-$ HEPs on day 4 and $CD43^+$ hematopoietic cells on day 12, differentiated from various hiPSC lines with/without transient GSKi treatment. 029L, 029G2 (a different clone of 029), SM28 (cord blood-derived), and TkDNSeV-2 (TkDN, embryonic fibroblast-derived) were used. Averages ($n = 3$) ± SD are provided ($^*p < 0.005$). (**C**) Hematopoietic colony assays. The 029L2 hiPSCs were differentiated with/without transient GSKi treatment. Whole cells were collected and cultured in MethoCult H4034. After 10 to 14 days, hematopoietic colonies were scored. Average numbers of colonies from 10^5 cells ($n = 3$) ± SD are provided ($^*p < 0.005$). Some colonies from day 12-induced cells were collected and stained with DiffQuick solution. *Arrowhead* indicates enucleated erythrocytes.

Hematopoietic differentiation following early GSKi treatment

The hematopoietic differentiation of hESCs/hiPSCs in vitro proceeds from $CD34^+CD43^-$ HEPs to $CD34^+CD43^+$ hematopoietic progenitor cells, followed by the appearance of $CD43^+CD45^+$ hematopoietic cells [18,19]. To determine whether early GSKi treatment affects HEP differentiation from hiPSCs, 029L2 hiPSCs were treated with or without a GSKi (days 0–1, 0–2, or 0–4), BMP-4 (days 1–4), and VEGF (days 2–4). Intriguingly, on day 4, the percentage of $CD34^+CD43^-$ HEPs increased dramatically from 0.2% to 19.8% following transient GSKi treatment (days 0–1) (Fig. 2D). GSKi treatment on day 0–2 was also effective for HEP induction, whereas continuous GSKi treatment was not (Fig. 2D). Consistent with previous data [20], continuous GSKi treatment augmented $CD184\ (CXCR4)^+$ endodermal progenitor production (Fig. 2D). Addition of a WNT inhibitor, Dkk1, inhibited GSKi-mediated HEP differentiation and EMT (Fig. 2E), suggesting that WNT upregulation by GSKi is responsible for the induction of HEP and EMT.

We next examined the effects of GSKi treatment (days 0–1) on the hematopoietic differentiation of hiPSCs. On day 4, a growth factor cocktail containing BMP4, SCF, FLT3L, IL-6, IL-3, and G-CSF [7] was added. On day 12, well-differentiated $CD43^+$ cells and a large number of $CD45^+$ cells were observed following GSKi treatment (Fig. 3A). In contrast, $CD43^+$ cells were barely detectable without GSKi treatment (Fig. 3A). Next, we examined whether the transient GSKi treatment is effective in other hiPSC lines. Expectedly, the GSKi treatment (days 0–1) significantly enhanced $CD34^+CD43^-$ HEP differentiation on day 4 and $CD43^+$ hematopoietic cell differentiation on day 12 in four different hiPSC lines, including TkDNSeV-2 [21] (Fig. 3B).

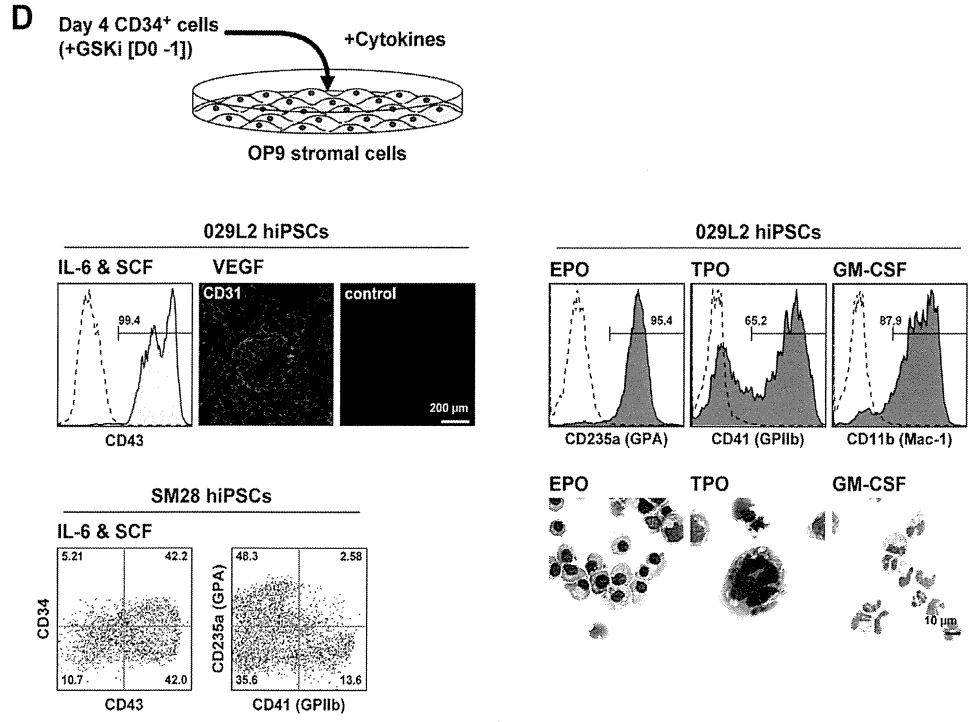

Figure 3. (*continued*) (**D**) Analyses of differentiation potentials of day 4 $CD34^+CD43^-$ HEPs. On day 4, HEPs from 029L2 and SM28 hiPSCs were isolated and cultured with OP9 cells for 10 to 16 days in the presence of cytokines, as indicated.

Colony assays revealed that 029L2 hiPSCs were differentiated into hematopoietic progenitor cells by GSKi (Fig. 3C). Notably, enucleated erythrocytes were detected, implying that these cells were derived from definitive hematopoiesis. These data proved that the transient GSKi treatment greatly promotes the hematopoietic differentiation of hiPSCs.

Hemogenic potential of GSKi-induced HEPs

To verify the hematopoietic/endothelial differentiation potential of the GSKi-induced $CD34^+CD43^-$ HEPs, we isolated these cells on day 4 and cultured them on OP9 stromal cells in the presence of various growth factors (Fig. 3D). When IL-6 and SCF were added, the HEPs produced $CD43^+$ hematopoietic cells (Fig. 3D). On the other hand, $CD31^+$ endothelial cells were produced from the HEPs when VEGF was added (Fig. 3D). Furthermore, when GSKi-induced HEPs were cultured on OP9 cells in the presence of erythropoietin (EPO), thrombopoietin (TPO), or granulocyte/macrophage colony-stimulating factor (GM-CSF), $CD235^+$ erythroid cells, $CD41^+$ megakaryocytes, and $CD11b^+$ myeloid cells were produced (Fig. 3D). Similar results were obtained when we used the SM28 hiPSC line. Therefore, GSKi-induced HEPs are capable of producing endothelial cells as well as multilineage hematopoietic cells.

According to the literature, enforced expression of *Cdx4* enhanced hematopoietic differentiation of mouse ESCs and in zebrafish [22,23]. In addition, it was recently reported that *HOXA9* promotes the hematopoietic differentiation of hESCs [24]. Thus, it is likely that these molecules are involved in the efficient induction of HEPs from hiPSCs by the transient GSKi treatment. In conclusion, we found that early GSKi treatment promotes the differentiation of hiPSCs into posterior mesoderm cells and activates *CDX/HOX* signaling, which facilitates the differentiation of hiPSCs into hematopoietic/endothelial cells. Our data highlight the pivotal role of WNT/β-CATENIN signaling in human embryonic hematopoietic development. Our in vitro hematopoietic induction system for hiPSCs faithfully recapitulates early human hematopoietic development, including PS, EMT, and posterior mesoderm induction.

Acknowledgments

This work was supported by Grants-in-Aid for Scientific Research from the Ministry of Education, Culture, Sports, Science, and Technology of Japan (24591415 to KK and 23390256 to KK and TH), a Grant-in-Aid for Research on Hepatitis from the Ministry of Health, Labour and Welfare, and the SENSHIN Medical Research Foundation.

We thank Dr. Koji Eto (Kyoto University) for kindly providing TkDNSeV-2 hiPSC line.

Author contributions

KK conceived the study, performed most of the experiments, and analyzed the data. MK and MN assisted with in vitro differentiation experiments. MK, AD, JT, MKS, MT, and AU established the hiPSC lines used in this study. KK and TH co-directed the project and wrote the article.

Conflict of interest disclosure

The authors declare no conflicts of interest.

References

1. Daley GQ, Scadden DT. Prospects for stem cell-based therapy. Cell. 2008;132:544–548.
2. Woll PS, Morris JK, Painschab MS, et al. Wnt signaling promotes hematoendothelial cell development from human embryonic stem cells. Blood. 2008;111:122–131.
3. Tan JY, Sriram G, Rufaihah AJ, et al. Efficient derivation of lateral plate and paraxial mesoderm subtypes from human embryonic stem cells through GSKi-mediated differentiation. Stem Cells Dev. 2013; 22:1893–1906.
4. Lian X, Bao X, Al-Ahmad A, et al. Efficient differentiation of human pluripotent stem cells to endothelial progenitors via small-molecule activation of WNT signaling. Stem Cell Rep. 2014;3:804–816.
5. Tam PP, Loebel DA, Tanaka SS. Building the mouse gastrula: Signals, asymmetry and lineages. Curr Opin Genet Dev. 2006;16:419–425.
6. Arkell RM, Fossat N, Tam PP. Wnt signalling in mouse gastrulation and anterior development: New players in the pathway and signal output. Curr Opin Genet Dev. 2013;23:454–460.
7. Chadwick K, Wang L, Li L, et al. Cytokines and BMP-4 promote hematopoietic differentiation of human embryonic stem cells. Blood. 2003;102:906–915.
8. Kitajima K, Tanaka M, Zheng J, et al. In vitro differentiation of mouse embryonic stem cells to hematopoietic cells on an OP9 stromal cell monolayer. Methods Enzymol. 2003;365:72–83.
9. Evseenko D, Zhu Y, Schenke-Layland K, et al. Mapping the first stages of mesoderm commitment during differentiation of human embryonic stem cells. Proc Natl Acad Sci U S A. 2010;107:13742–13747.
10. Takahashi K, Tanabe K, Ohnuki M, et al. Induction of pluripotent stem cells from adult human fibroblasts by defined factors. Cell. 2007;131: 861–872.
11. Deschamps J, van Nes J. Developmental regulation of the Hox genes during axial morphogenesis in the mouse. Development. 2005;132: 2931–2942.
12. Kinder SJ, Tsang TE, Wakamiya M, et al. The organizer of the mouse gastrula is composed of a dynamic population of progenitor cells for the axial mesoderm. Development. 2001;128:3623–3634.
13. Lian X, Hsiao C, Wilson G, et al. Robust cardiomyocyte differentiation from human pluripotent stem cells via temporal modulation of canonical Wnt signaling. Proc Natl Acad Sci U S A. 2012;109:E1848–E1857.
14. Lengerke C, Schmitt S, Bowman TV, et al. BMP and Wnt specify hematopoietic fate by activation of the Cdx–Hox pathway. Cell Stem Cell. 2008;2:72–82.
15. Pilon N, Oh K, Sylvestre JR, et al. Cdx4 is a direct target of the canonical Wnt pathway. Dev Biol. 2006;289:55–63.
16. Pilon N, Oh K, Sylvestre JR, et al. Wnt signaling is a key mediator of Cdx1 expression in vivo. Development. 2007;134:2315–2323.
17. Gadue P, Huber TL, Nostro MC, et al. Germ layer induction from embryonic stem cells. Exp Hematol. 2005;33:955–964.
18. Vodyanik MA, Bork JA, Thomson JA, et al. Human embryonic stem cell-derived CD34+ cells: Efficient production in the coculture with OP9 stromal cells and analysis of lymphohematopoietic potential. Blood. 2005;105:617–626.
19. Choi KD, Vodyanik M, Slukvin II. Hematopoietic differentiation and production of mature myeloid cells from human pluripotent stem cells. Nat Protoc. 2011;6:296–313.
20. Bone HK, Nelson AS, Goldring CE, et al. A novel chemically directed route for the generation of definitive endoderm from human embryonic stem cells based on inhibition of GSK-3. J Cell Sci. 2011;124: 1992–2000.
21. Davidson AJ, Ernst P, Wang Y, et al. cdx4 mutants fail to specify blood progenitors and can be rescued by multiple hox genes. Nature. 2003; 425:300–306.
22. Nakamura S, Takayama N, Hirata S, et al. Expandable megakaryocyte cell lines enable clinically applicable generation of platelets from human induced pluripotent stem cells. Cell Stem Cell. 2014; 14:535–548.
23. McKinney-Freeman SL, Lengerke C, Jang IH, et al. Modulation of murine embryonic stem cell-derived CD41+c-kit+ hematopoietic progenitors by ectopic expression of Cdx genes. Blood. 2008;111: 4944–4953.
24. Ramos-Mejøía V, Navarro-Montero O, Ayllón V, et al. HOXA9 promotes hematopoietic commitment of human embryonic stem cells. Blood. 2014;124:3065–3075.

© 2015. Published by The Company of Biologists Ltd | Development (2015) 142, 4049-4055 doi:10.1242/dev.127308

RESEARCH REPORT

Chromatin condensation of *Xist* genomic loci during oogenesis in mice

Atsushi Fukuda[1], Atsushi Mitani[1,2], Toshiyuki Miyashita[2], Akihiro Umezawa[1] and Hidenori Akutsu[1,3,*]

ABSTRACT

Repression of maternal *Xist* (Xm-*Xist*) during preimplantation in mouse embryos is essential for establishing imprinted X chromosome inactivation. Nuclear transplantation (NT) studies using nuclei derived from non-growing (ng) and full-grown (fg) oocytes have indicated that maternal-specific repressive modifications are imposed on Xm-*Xist* during oogenesis, as well as on autosomal imprinted genes. Recent studies have revealed that histone H3 lysine 9 trimethylation (H3K9me3) enrichments on Xm-*Xist* promoter regions are involved in silencing at the preimplantation stages. However, whether H3K9me3 is imposed on Xm-*Xist* during oogenesis is not known. Here, we dissected the chromatin states in ng and fg oocytes and early preimplantation stage embryos. Chromatin immunoprecipitation experiments against H3K9me3 revealed that there was no significant enrichment within the Xm-*Xist* region during oogenesis. However, NT embryos with ng nuclei (ngNT) showed extensive Xm-*Xist* derepression and H3K9me3 hypomethylation of the promoter region at the 4-cell stage, which corresponds to the onset of paternal *Xist* expression. We also found that the chromatin state at the *Xist* genomic locus became markedly condensed as oocyte growth proceeded. Although the condensed Xm-*Xist* genomic locus relaxed during early preimplantation phases, the extent of the relaxation across Xm-*Xist* loci derived from normally developed oocytes was significantly smaller than those of paternal-*Xist* and ngNT-*Xist* genomic loci. Furthermore, Xm-*Xist* from 2-cell metaphase nuclei became derepressed following NT. We propose that chromatin condensation is associated with imprinted *Xist* repression and that skipping of the condensation step by NT leads to *Xist* activation during the early preimplantation phase.

KEY WORDS: *Xist*, Imprinted XCI, Chromatin condensation, Oogenesis, Histone methylation, Nuclear transfer

INTRODUCTION

Expression of the large non-coding RNA X inactive specific transcript (*Xist*) is essential for the initiation of X chromosome inactivation (XCI) in female mice and humans (Augui et al., 2011; Sado and Sakaguchi, 2013; Lee, 2011). In mice, *Xist* expression is initiated around the 4-cell stage and is restricted to the paternal allele (Augui et al., 2011; Sado and Sakaguchi, 2013; Nesterova et al., 2001). This expression pattern leads to the establishment of imprinted XCI in extra-embryonic tissues (Takagi and Sasaki, 1975). Paternal *Xist* (Xp-*Xist*) expression is driven by the deposition of maternal Rnf12 (also known as Rlim – Mouse Genome Informatics) (Shin et al., 2010; Jonkers et al., 2009). However, the *Xist* locus on the maternal X chromosome (Xm) is tightly protected by epigenetic factors. Using parthenogenetic embryos, which are composed of two maternal genomes, we previously demonstrated that histone 3 lysine 9 trimethylation (H3K9me3) is essential for Xm-*Xist* repression during early preimplantation phases (Fukuda et al., 2014).

Using a nuclear transplantation (NT) technique, bi-maternal embryos were constructed from non-growing (ng) and fully grown (fg) oocytes (Kono et al., 1996). XCI in the extra-embryonic tissues of bi-maternal embryos predominantly occurred on the allele from ng oocytes (Tada et al., 2000). The results indicated that the *Xist* loci of ng oocytes are in specifically permissive states for activation and that Xm-*Xist* imprints are established during oogenesis, as are those of autosomal imprinted genes. However, Xm-*Xist* silencing was observed in primordial germ cells (Sugimoto and Abe, 2007), suggesting that *in vivo*, repressive modifications were already imposed on the Xm-*Xist* prior to oogenesis. In addition, *Xist* dysregulation commonly occurred in cloned mouse embryos from various cell types such as somatic and embryonic stem cells (Inoue et al., 2010; Fukuda et al., 2010). Considering that NT is an artificial system, it does not exclude the possibility that NT embryos might not be faithfully reprogrammed. Therefore, in the present study we scrutinised the regulation of Xm-*Xist* by H3K9me3 and chromatin state in NT embryos derived from ng oocytes (ngNT).

RESULTS AND DISCUSSION

H3K9me3 is comparable between ng and fg oocytes at Xm-*Xist* loci

We initially confirmed that Rnf12 is highly expressed during oogenesis (Fig. S1), as described elsewhere (Shin et al., 2010), indicating that the *Xist* repressive state is established prior to oocyte maturation. We previously demonstrated that H3K9me3 is essential for Xm-*Xist* repression in preimplantation embryos (Fukuda et al., 2014). To examine the chromatin states at *Xist* loci, we used an advanced system of embryo chromatin immunoprecipitation combined with TaqMan gene expression (eChIP-qPCR), which facilitated chromatin analysis of many loci from small numbers of cells. We targeted 19 regions in the *Xist* genes containing promoter regions and a *Gapdh* promoter region as a negative control region for H3K9me3 modification. Our eChIP-qPCR system robustly correlated with the conventional method (no preamplification) (1.21 to 1.57-fold increase in eChIP-qPCR, correlation between the two methods was >0.96; Fig. S2). We therefore examined H3K9me3 in ng and fg oocytes. eChIP-qPCR in ng oocytes revealed that the H3K9me3 levels of the 19 *Xist* regions examined were markedly

[1]Center for Regenerative Medicine, National Research Institute for Child Health and Development, 2-10-1 Okura, Setagaya, Tokyo 157-8535, Japan. [2]Department of Molecular Genetics, Kitasato University Graduate School of Medical Sciences, 1-15-1 Kitasato, Minami, Sagamihara, Kanagawa 252-0374, Japan. [3]Department of Stem Cell Research, Fukushima Medical University, 1 Hikarigaoka, Fukushima City, Fukushima 960-1295, Japan.

*Author for correspondence (akutsu-h@ncchd.go.jp)

Received 11 June 2015; Accepted 2 October 2015

Development (2015) 142, 4049-4055 doi:10.1242/dev.127308

higher than that of the *Gapdh* promoter region (Fig. 1); specifically, the levels in the *Xist* promoter regions were up to 6-fold higher. The repressive states across the entire *Xist* region were maintained in fg oocytes, and there were no significant differences between ng and fg oocytes in H3K9me3 levels at any of the *Xist* regions analysed (Fig. 1). These results indicated that transcriptional repressive states were imposed by H3K9me3 in ng oocytes and that the modifications were not established during oogenesis.

Specific loss of H3K9me3 at Xm-*Xist* promoter regions following NT

Our findings showed that the *in vivo* repressive histone H3K9me3 modifications were already imposed on Xm-*Xist* prior to the initiation of oogenesis. Generally, immunofluorescence (IF) analysis showed that after fertilisation, global H3K9me3 was specifically imposed on the maternal genome (Santos et al., 2005; Kageyama et al., 2007). Interestingly, the lack of H3K9me3 was not restricted to the sperm genome. IF analysis revealed that global H3K9me3 levels at the 1-cell stage were markedly lower in the genomes from somatic and embryonic stem cells (ESCs) compared with maternal genomes (Wang et al., 2007) (Fig. S3A). However, the dramatically low H3K9me3 levels in ESCs and sperm genomes were not observed at the 2- and 4-cell stages (Fig. S3B). These observations implied that the relaxed chromatin state characterised by low H3K9me3 levels at the 1-cell stage might be important for subsequent *Xist* expression in early preimplantation phases.

To ascertain chromatin states, we constructed NT embryos with ng oocyte genomes (ngNT) and performed IF analysis against H3K9me3. We first examined whether the Xm-*Xist* of ngNT was derepressed at the 4-cell stage. Fluorescence *in situ* hybridisation (FISH) analysis for *Xist* RNA showed extensive *Xist* expression (Fig. 2A), confirming that derepression of Xm-*Xist* in ngNT commenced at early preimplantation phases. Next, we conducted IF analysis for H3K9me3 at the 1-cell stage in ngNT constructed by serial NT (Kawahara et al., 2008). Unexpectedly, compared with control embryos (fgNT), there were no apparent reductions in H3K9me3 modifications in ngNT, and the same modifications were observed at the 1-cell to 4-cell stage (Fig. 2B). The signals of H3K9me3 in ngNT and fgNT were significantly higher than those of fertilised embryos (IVF, parental genomes; Fig. 2B), consistent with a previous report that Ring1b (also known as Rnf2 – Mouse Genome Informatics) – but not H3K9me3 – is enriched in paternal constitutive heterochromatin (Puschendorf et al., 2008).

We also examined the expression states of H3K9me3-associated genes (Peters et al., 2001; Matsui et al., 2010; Greer and Shi, 2012; Klose and Zhang, 2007) (erasers: *Kdm4a/b/c*, writers: *Suv39h1/2*, *Setdb1*) at the 4-cell stage of ngNT and found that the expression levels varied among the ngNT, as well as between control group embryos (Fig. S3C). Although only *Kdm4a* was markedly reduced in most ngNT, it did not seem to affect H3K9me3. These results indicated that global ng genomic H3K9me3 following NT was comparable to that of the fg oocyte genome.

However, a previous study has shown Xm-*Xist* activation to be accompanied by promoter demethylation (Fukuda et al., 2014). Thus, we next asked whether Xm-*Xist* derepression of ngNT embryos at the 4-cell stage could be attributed to the loss of H3K9me3 at *Xist* promoter regions. To reduce the number of embryos required for eChIP-qPCR analysis, we constructed tetraploid ngNT by repressing second polar body release. The tetraploid ngNT also showed Xm-*Xist* derepression at the 4-cell stage (Fig. S4). As expected, H3K9me3 modifications at *Xist* major promoter regions in tetraploid ngNTs at the 4-cell stage declined dramatically (less than 15% of the control) (Fig. 2C). The A repeat regions showed slight demethylation (around 60% of control), consistent with previous results of H3K9me3 demethylase-mediated Xm-*Xist* derepression (Fukuda et al., 2014). Thus, intrinsic Xm-*Xist* protection by H3K9me3 was not maintained following NT.

Genome-wide loss of H3K9me2 in ngNT embryos at the 1-cell stage

We further examined H3K9me2 and H3K27me3 in ngNT embryos because both were shown to be specifically imposed on maternal genomes in zygotes (Fukuda et al., 2014; Santos et al., 2005; Nakamura et al., 2012). H3K27me3 levels of ng and fg oocyte genomes were comparable (Fig. S5A). However, H3K9me2 signals in ngNT were much lower than those in fgNT (Fig. S5A), although low levels of global H3K9me2 were only observed at the 1-cell stage, with no apparent differences at the 2- and 4-cell stages (Fig. S5B). Although the loss of H3K9me2 in the maternal genome did not affect Xm-*Xist* derepression (Fukuda et al., 2014),

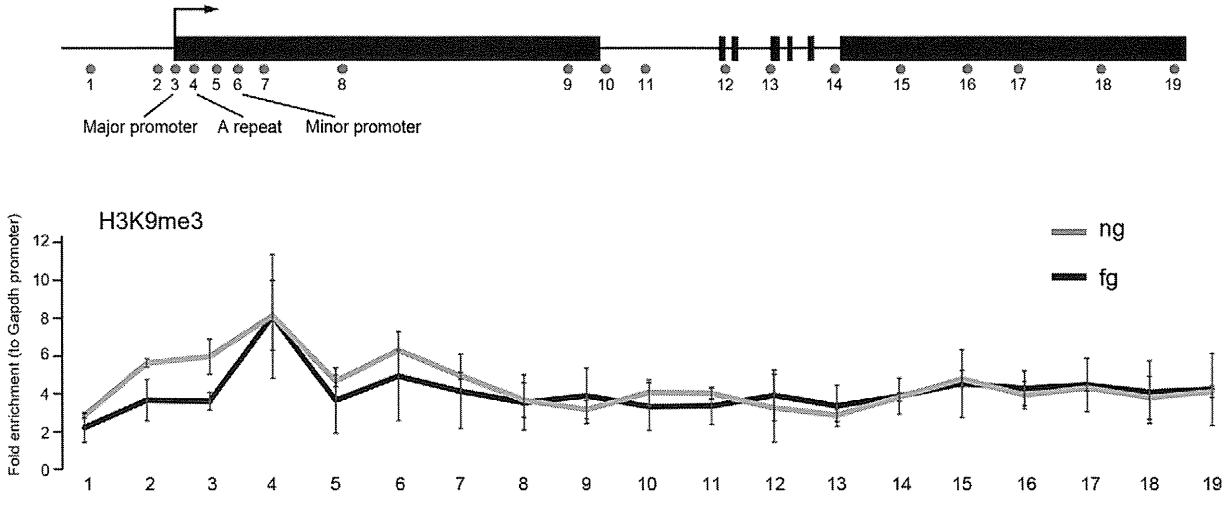

Fig. 1. H3K9me3 states in ng and fg oocytes by eChIP-qPCR analysis. A total of 19 regions in *Xist* were analysed by eChIP-qPCR. Positions 3, 4, and 6 were localised in the major promoter, A repeat, and minor promoter, respectively. There were no significant differences among the regions tested. Three independent experiments were carried out, and the error bars show the standard error of the mean (s.e.m.).

Development (2015) 142, 4049-4055 doi:10.1242/dev.127308

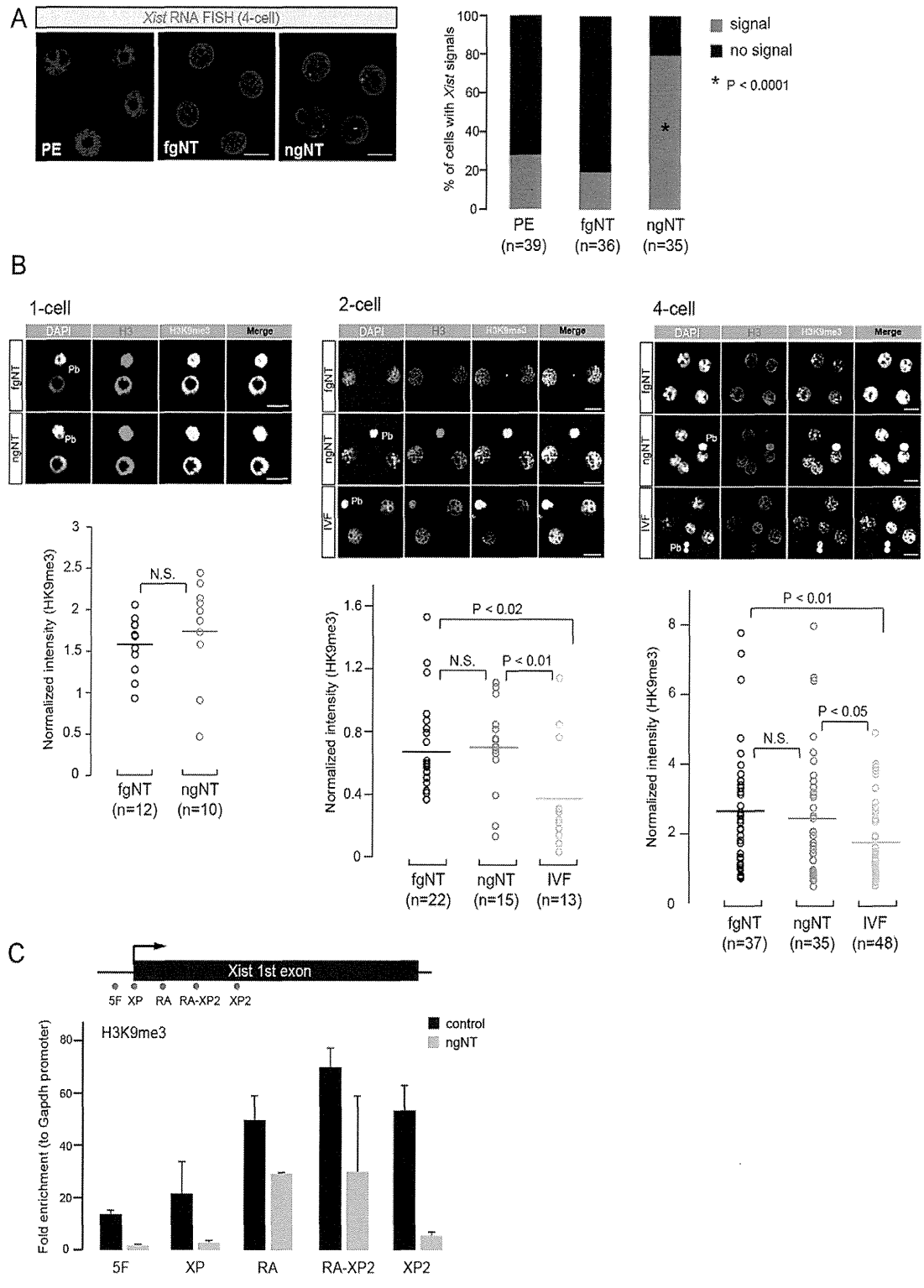

Fig. 2. Loss of H3K9me3 in ngNT embryos at Xm-*Xist* promoter regions but not genome wide. (A) *Xist* RNA-FISH analysis at the 4-cell stage of ngNT (diploid ng genomes), fgNT (diploid fg genomes), and parthenogenetic (diploid fg genomes) embryos. Nuclei stained with 4′,6-diamidino-2-phenylindole (DAPI) are shown in blue. *Xist* is shown in red. *n*=number of analysed nuclei. The *P*-values were calculated using Fisher's exact test (compared with PE and fgNT, respectively). (B) IF analysis of H3K9me3 in ngNT embryos and control (fgNT) embryos constructed by serial NT at the 1-cell stage. fgNT and ngNT embryos were produced by single NT at 2- and 4-cell stages. For comparison with fertilised embryos, *in vitro* fertilised (IVF) embryos were prepared. *n*=number of analysed nuclei. Scale bar: 20 µm. DAPI, white; H3, red; H3K9me3, green. Pb, polar body. The H3K9me3 signal intensity was normalised by the H3 signal. *P*-values were calculated using Student's *t*-test. N.S., not significant. (C) eChIP-qPCR analysis of ngNT and control (tetraploid fgNT) embryos at the 4-cell stage. H3K9me3 at Xm-*Xist* promoter regions of tetraploid embryos in both groups were analysed by eChIP-qPCR. Two independent experiments were conducted, and error bars show s.e.m.

given that H3K9me2 is inversely related to gene expression at a genome-wide scale (Wen et al., 2009), the genome-wide lack of H3K9me2 at the 1-cell stage suggested that the chromatin of ng oocytes might be loosened following NT.

Chromatin condensation of *Xist* genomic loci during oogenesis and relaxation in early preimplantation

Consistent with the above notion, DNA methylation levels were shown to dramatically change during oogenesis, and high levels of

Development (2015) 142, 4049-4055 doi:10.1242/dev.127308

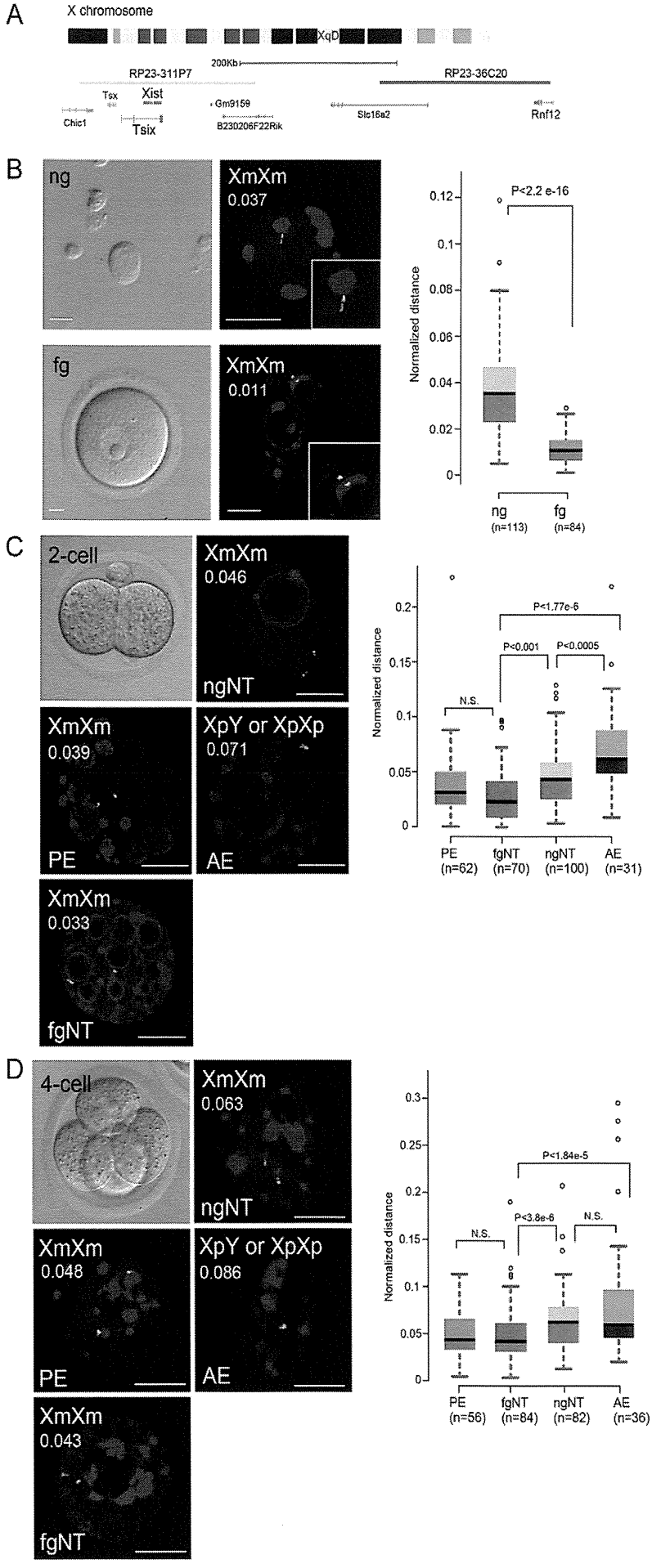

Fig. 3. DNA FISH analysis at the *Xist* genomic loci in ng and fg oocytes and various preimplantation embryos. (A) Measurement of the distance between centroids of each signal by DNA-FISH using BAC clones. The BAC clone colours, green for RP23-311P7 and red for RP23-36C20, correspond with the signals in B-D. (B-D) DNA-FISH analysis in ng and fg oocytes (B) and in parthenogenetic (PE: diploid fg genomes), fgNT (diploid fg genome), ngNT (diploid ng genomes), and androgenetic (AE: diploid sperm genomes) embryos at 2-cell (C) and 4-cell (D) stages. *n*=number of analysed signals. The boxplot indicates the normalised distances, and *P*-values were calculated by Mann–Whitney *U*-tests. Xm, maternal X chromosome; Xp, paternal X chromosome. Scale bar: 10 µm. Nuclei (DAPI), blue. Average values of normalised distance are given top left in each image.

Development (2015) 142, 4049-4055 doi:10.1242/dev.127308

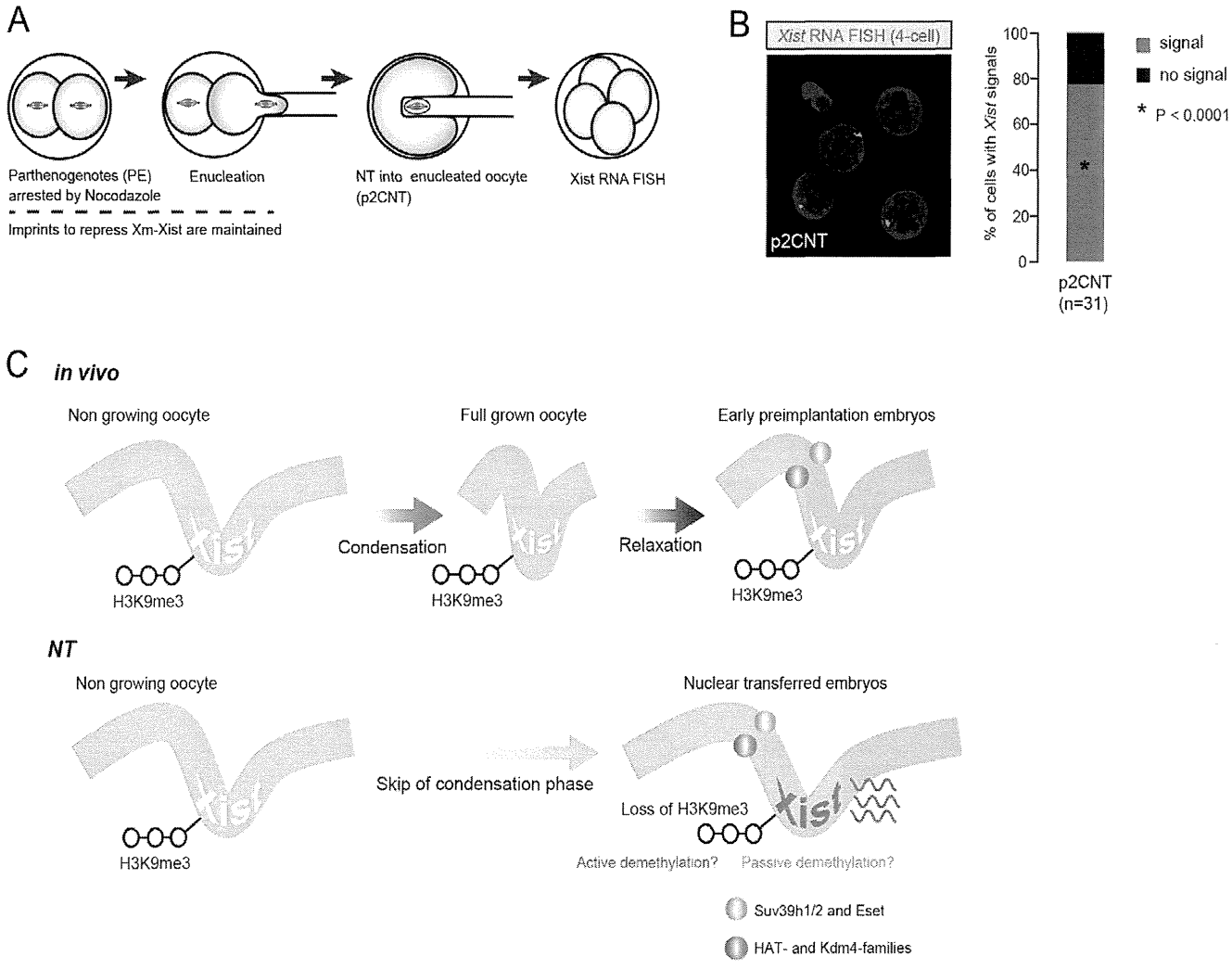

Fig. 4. Imprinted Xm-*Xist* silencing in early embryonic nuclei are not reprogrammed following NT. (A) Experimental scheme of embryonic NT. Diploid parthenogenetic 2-cell embryos were incubated in the presence of Nocodazol (0.1 µg/ml) for 12 h and washed in M2 medium to form spindles. Condensed nuclei of metaphase-arrested 2-cell parthenogenotes (PE) were transferred into enucleated oocytes (p2CNTs). (B) *Xist* RNA-FISH analysis of p2CNT embryos at the 4-cell stage. The bar graph shows the *Xist* expression states in each embryo. *P*-values were calculated by Fisher's exact tests in comparison with the PE and fgNT embryos in Fig. 2A. (C) Model of Xm-*Xist* silencing machinery from oogenesis to early preimplantation phases. During oogenesis, Xm-*Xist* loci are condensed, but become relaxed in early preimplantation phases. NT skips the condensation phase to result in Xm-*Xist*, which is in a permissive state for activation. During oocyte and early preimplantation stages, some H3K9me3 demethylases and histone acetylases are expressed (Fukuda et al., 2014; Yoshida et al., 2007). Open chromatin might cause active or passive demethylation.

DNA methylation were observed only in fg oocyte genomes (Shirane et al., 2013). We speculated that maternal genomes might become transcriptionally silent via chromatin condensation. To test this, we carried out DNA-FISH experiments using probes spanning XqD, which contains *Xist*, and measured the distance between loci (Fig. 3A). Many studies have normalised distance with this method by calculating the nuclear radius visualised by 4′,6-diamidino-2-phenylindole (DAPI) staining (Terranova et al., 2008; Eskeland et al., 2010; Chambeyron and Bickmore, 2004). However, the chromatin in fg oocytes surrounds the nucleolus, and the DAPI-positive area does not totally cover the regions enclosed by the nuclear membrane (De La Fuente, 2006). Therefore, to determine accurate nuclear radii in fg oocytes, we conducted IF against histone deacetylase 2 (Hdac2), which occurs specifically in the nuclear area. Furthermore, a report has shown the predominant expression of Hdac2 in fg oocytes during oogenesis (Fig. S6A) (Ma et al., 2012). The distance in the fg oocyte genome was therefore normalised by the average radius, whereas the distance of the ng oocyte genome was normalised by the DAPI-positive nuclear area (average of ng oocyte examined). DNA-FISH analysis showed that the genomic regions containing *Xist* were significantly condensed in fg oocytes even without normalisation (Fig. 3B, Fig. S6B), indicating that the chromatin of the *Xist* genomic locus became condensed during oogenesis.

Next, we conducted DNA-FISH experiments at the 2- and 4-cell stages in ngNT, parthenogenetic (derived from fg oocytes), and androgenetic embryos (containing *Xist* genomic loci derived from paternal X chromosomes). At the 2-cell stage, the distance between loci in ngNT embryos was significantly larger than that of parthenogenetic and fgNT embryos, but smaller than that of androgenetic embryos (Fig. 3C). However, at the 4-cell stage, the distance was comparable to that of androgenetic embryos but significantly larger than that of parthenogenetic and fgNT embryos (Fig. 3D). Thus, the open chromatin state in ng oocytes was maintained following NT, suggesting that chromatin condensation is likely essential for *Xist* repression.

Imprinted Xm-*Xist* silencing in early embryonic cells is not reprogrammed following NT

We also found that the distance between *Xist* genomic loci became larger following cell division (Fig. 3B-D), implying that chromatin

Development (2015) 142, 4049-4055 doi:10.1242/dev.127308

becomes gradually relaxed during the early cleavage stage, probably reflecting zygotic gene activation. Thus, we hypothesised that although 4-cell stage parthenogenetic embryo Xm-*Xist* was silenced, the chromatin might be looser than in fg oocytes and thus might be derepressed following NT. We therefore produced 2-cell parthenogenotes arrested at metaphase by Nocodazol treatment and conducted NT experiments (Egli et al., 2009) (Fig. 4A). *Xist* RNA-FISH revealed that Xm-*Xist* of NT embryos derived from arrested nuclei of 2-cell parthenogenotes (wherein imprinted *Xist* silencing was maintained) was robustly expressed at the 4-cell stage (77% of nuclei; Fig. 4B). These results indicated that imprinted *Xist* repression associated with open chromatin states in donor cells was not faithfully reprogrammed following NT.

Conclusions

As imprinted *Xist* expression is not common in other species, the observed genome condensation during oogenesis might specifically occur on the murine X chromosome. Accordingly, we found that X-linked gene expression levels in mice markedly declined during oogenesis, whereas they were only slightly reduced in mature human oocytes (Fukuda et al., 2015).

NT studies in mice showed *Xist* upregulation regardless of donor cell origins (Fukuda et al., 2010), even if the *Xist* imprint was maintained in donor cells such as from early preimplantation embryos (Fig. 4B). Furthermore, considering that H3K9me3 demethylases and histone acetyltransferases are expressed in oocytes (Fukuda et al., 2014; Yoshida et al., 2007), the Xm-*Xist* promoter in ngNT could be subjected to demethylation owing to chromatin decondensation (Fig. 4C). Overall, our results suggest – as previously proposed by Sado and Sakaguchi (2013) – that chromatin condensation is associated with imprinted *Xist* repression on the maternal X at the early preimplantation stage, and that skipping of the condensation step by NT leads to precocious activation of *Xist* in early preimplantation embryos.

MATERIALS AND METHODS

Animals

All mice were maintained and used in accordance with the Guidelines for the Care and Use of Laboratory Animals of the Japanese Association for Laboratory Animal Science and the National Research Institute for Child Health and Development of Japan (A2006-009-C09).

Oocyte and sperm collection

Female B6D2F1 and C57BL/6N mice were purchased from Clea Japan, and oocytes were collected following standard methods. The ng and fg oocytes (C57BL/6N) were recovered from new-born (1- to 5-day-old) and adult (8- to 12-week-old) mice according to previous reports (Kawahara et al., 2008). For eChIP-qPCR analysis, ng oocytes were collected using a micromanipulator. Sperm was collected from male B6D2F1 (8-16 weeks) mice according to reported methods (Fukuda et al., 2014).

Embryo manipulations

Parthenogenetic embryos were generated using calcium-free M16 medium containing 8 mM $SrCl_2$ and 5 µg/ml cytochalasin B (Sigma-Aldrich) (activation medium) and were cultured in KSOM (EMD Millipore). Serial NT of ng oocytes for immunofluorescence analysis was conducted as described (Kawahara et al., 2008). Single NT for ng oocyte nuclei was conducted using a Piezo drive (Sutter Instrument Company) or hemagglutinating virus of Japan envelope (HVJ-E; Ishihara Sangyo Kaisha) (Kawahara et al., 2008; Egli et al., 2009). To produce diploid ngNT embryos for DNA FISH analysis, cytochalasin B was removed from the activation medium, whereas tetraploid ngNT embryos were generated by adding cytochalasin B to the activation medium. For construction of tetraploid fgNT, an MII oocyte received a nucleus from another MII oocyte by NT and then the NT embryo was parthenogenetically activated in the presence of cytochalasin B. The diploid androgenetic embryos were generated using a previously reported method (Kono et al., 1993). For ESC injection, ovulated MII oocytes at 12-13 h after human chorionic gonadotropin (hCG) injection were recovered to retain the first polar body, and ESCs were injected using the Piezo drive. All embryos were cultured at 37°C in KSOM in an atmosphere containing 5% CO_2.

Fluorescence *in situ* hybridisation (FISH)

RNA-FISH analysis was performed according to a previous report (Fukuda et al., 2014). In brief, an *Xist* probe (provided by T. Sado) was prepared using a Nick Translation Kit (Abbott Laboratories) and Cy3-dUTP (GE Healthcare Life Sciences).

For DNA-FISH, BAC clones (RP23-311P7: *Xist/Tsix* regions and RP23-36C20: *Slc16a2/Rnf12* regions) were purchased from Life Technologies. DNA probes of RP23-311P7 and RP23-36C20 were prepared using the Nick Translation Kit with Cy5-dUTP and Cy3-dUTP, respectively. The procedures were as previously reported. In brief, fixation (2% paraformaldehyde) and permeabilisation (0.25% Triton X-100) were simultaneously conducted for 5 min at room temperature, and then the samples were plated onto glass slides. After RNaseA treatment, the samples were incubated in 0.2 N HCl containing 0.5% Triton X-100 on ice for 10 min. The images were obtained by LSM510 laser scanning confocal microscopy using a Plan-Apochromat 100×/1.46 Oil DIC objective (Carl Zeiss).

Distance measurements were based on previous reports (Terranova et al., 2008; Eskeland et al., 2010; Chambeyron and Bickmore, 2004). Briefly, the signal centroid was calculated by NIH ImageJ software (http://rsb.info.nih.gov/ij/). Each nuclear radius, except for those of fg oocytes, used for distance normalisation was calculated using the DAPI-stained area measurement.

eChIP-qPCR for oocytes and embryos

We prepared 300 fg and ng oocytes and 50 tetraploid 4-cell embryos for the eChIP-qPCR assay. Zona pellucida-free fg oocytes, embryos and ng oocytes were suspended in PBS containing 0.5% Triton-X100, 0.5 mM DTT and protease inhibitor (PBS + lysis buffer) and incubated on ice for 30 min. The chromatin was incubated with 100 Gel U/µl micrococcal nuclease (final 0.33 Gel U) (New England BioLabs) for 5 min at 37°C, after which the chromatin was extracted by centrifugation. After recovery of the supernatant, PBS + lysis buffer was added to the (invisible) pellet, and an additional treatment with 2000 Gel U/µl micrococcal nuclease (final 6.7 Gel U) for 5 min at 37°C was performed. The chromatin was then incubated with an antibody against H3K9me3 (Abcam, ab8898) conjugated with protein A (Dynabeads) overnight at 4°C. The pelleted beads were washed twice with both Buffer 1 (50 mM Tris-HCl pH 7.5, 500 mM NaCl, 10 mM EDTA) and Buffer 2 (50 mM Tris-HCl pH 7.5, 300 mM NaCl, 10 mM EDTA). The pelleted beads were suspended in ChIP direct elution buffer (Nippon Gene) and incubated with proteinase K for 2 h at 37°C (Roche). The immunoprecipitated DNA was then purified using Agencourt AMpure XP beads (Beckman). The DNA was preamplified using the preamplification mix from the Single Cell-to-CT Kit (Ambion) and TaqMan probes according to the manufacturer's instructions (except that the number of PCR cycles was changed to 20). The primers/probes used are listed in Table S1.

Immunofluorescence

The antibodies for H3K9me2 (Abcam, ab1220), H3K9me3 (Abcam, ab8898), H3K27me3 (Millipore, 07-449), H3 (Active Motif, 39763) and Hdac2 (Millipore, 05-814) were used for immunofluorescence (IF) analysis. For IF against histone methylation, fixation by 2% paraformaldehyde and permeabilisation with 0.25% Triton X-100 were simultaneously conducted. Fixation was followed by permeabilisation for Hdac2 IF analysis. After fixation and permeabilisation the embryos were blocked in PBS containing 1% BSA (blocking buffer) for 1 h and incubated with antibodies overnight at 4°C. The first antibodies for H3K9me2 (1:500) and H3K27me3 (1:300), or H3 (1:500) and H3K9me3 (1:500), were simultaneously incubated in blocking buffer. Embryos were washed with PBS containing 0.1% polyvinyl alcohol (PBS-PVA) and then incubated for 1 h at room temperature with

Alexa Fluor 488- or 546-conjugated anti-mouse or anti-rabbit IgG secondary antibodies (Life Technologies; 1:500). After the embryos were washed with PBS-PVA, the nuclei were stained with DAPI. The zona pellucida was removed prior to fixation and permeabilisation (Fig. 2B). After the second antibodies were washed, the samples were attached onto slide glasses and observed.

qPCR analysis of 4-cell stage embryos

The qPCR analysis was conducted using TaqMan probes (Life Technologies). For further details, see the supplementary Materials and Methods and Table S2.

ESC culture

The culture of ESCs used for NT was according to a previous report (Fukuda et al., 2014). For further details, see the supplementary Materials and Methods.

Acknowledgements

We are grateful to Dr T. Sado (Kinki University, Japan) for the initial proposal of the genomic condensation study, critical reading of the manuscript, and helpful comments. We also thank T. Takigashira and T. Kawasaki for microscopic observation studies and preparation of the figures, respectively.

Competing interests

The authors declare no competing or financial interests.

Author contributions

A.F. and H.A. conceived the idea. A.F. designed the experiments. A.F. and A.M. conducted all experiments and data analysis. A.U., T.M. and H.A. generated materials and provided analytic tools. H.A. supervised the study. A.F. and H.A. wrote the manuscript.

Funding

This work was supported by grants from the Ministry of Education, Culture, Sports, Science, and Technology (MEXT) of Japan; a grant from the Ministry of Health, Labor, and Welfare (MHLW) to H.A. and A.U.; a Grant-in-Aid for Scientific Research [21390456]; a grant from JST-CREST to H.A.; and a JSPS KAKENHI Grant-in-Aid for Young Scientists (B) to A.F. [26861350]. Deposited in PMC for immediate release.

Supplementary information

Supplementary information available online at
http://dev.biologists.org/lookup/suppl/doi:10.1242/dev.127308/-/DC1

References

Augui, S., Nora, E. P. and Heard, E. (2011). Regulation of X-chromosome inactivation by the X-inactivation centre. *Nat. Rev. Genet.* **12**, 429-442.

Chambeyron, S. and Bickmore, W. A. (2004). Chromatin decondensation and nuclear reorganization of the HoxB locus upon induction of transcription. *Genes Dev.* **18**, 1119-1130.

De La Fuente, R. (2006). Chromatin modifications in the germinal vesicle (GV) of mammalian oocytes. *Dev. Biol.* **292**, 1-12.

Egli, D., Sandler, V. M., Shinohara, M. L., Cantor, H. and Eggan, K. (2009). Reprogramming after chromosome transfer into mouse blastomeres. *Curr. Biol.* **19**, 1403-1409.

Eskeland, R., Leeb, M., Grimes, G. R., Kress, C., Boyle, S., Sproul, D., Gilbert, N., Fan, Y., Skoultchi, A. I., Wutz, A. et al. (2010). Ring1B compacts chromatin structure and represses gene expression independent of histone ubiquitination. *Mol. Cell* **38**, 452-464.

Fukuda, A., Cao, F., Morita, S., Yamada, K., Jincho, Y., Tane, S., Sotomaru, Y. and Kono, T. (2010). Identification of inappropriately reprogrammed genes by large-scale transcriptome analysis of individual cloned mouse blastocysts. *PLoS ONE* **5**, e11274.

Fukuda, A. Tomikawa, J., Miura, T., Hata, K., Nakabayashi, K., Eggan, K., Akutsu, H. and Umezawa, A. (2014). The role of maternal-specific H3K9me3 modification in establishing imprinted X-chromosome inactivation and embryogenesis in mice. *Nat. Commun.* **5**, 5464.

Fukuda, A., Tanino, M., Matoba, R., Umezawa, A. and Akutsu, H. (2015). Imbalance between the expression dosages of X-chromosome and autosomal genes in mammalian oocytes. *Sci. Rep.* **5**, 14101.

Greer, E. L. and Shi, Y. (2012). Histone methylation: a dynamic mark in health, disease and inheritance. *Nat. Rev. Genet.* **13**, 343-357.

Inoue, K., Kohda, T., Sugimoto, M., Sado, T., Ogonuki, N., Matoba, S., Shiura, H., Ikeda, R., Mochida, K., Fujii, T. et al. (2010). Impeding Xist expression from the active X chromosome improves mouse somatic cell nuclear transfer. *Science* **330**, 496-499.

Jonkers, I. Barakat, T. S., Achame, E. M., Monkhorst, K., Kenter, A., Rentmeester, E., Grosveld, F., Grootegoed, J. A. and Gribnau, J. (2009). RNF12 is an X-Encoded dose-dependent activator of X chromosome inactivation. *Cell* **139**, 999-1011.

Kageyama, S.-I., Liu, H., Kaneko, N., Ooga, M., Nagata, M. and Aoki, F. (2007). Alterations in epigenetic modifications during oocyte growth in mice. *Reproduction* **133**, 85-94.

Kawahara, M., Obata, Y., Sotomaru, Y., Shimozawa, N., Bao, S., Tsukadaira, T., Fukuda, A. and Kono, T. (2008). Protocol for the production of viable bimaternal mouse embryos. *Nat. Protoc.* **3**, 197-209.

Klose, R. J. and Zhang, Y. (2007). Regulation of histone methylation by demethylimination and demethylation. *Nat. Rev. Mol. Cell Biol.* **8**, 307-318.

Kono, T., Sotomaru, Y., Sato, Y. and Nakahara, T. (1993). Development of androgenetic mouse embryos produced by in vitro fertilization of enucleated oocytes. *Mol. Reprod. Dev.* **34**, 43-46.

Kono, T., Obata, Y., Yoshimzu, T., Nakahara, T. and Carroll, J. (1996). Epigenetic modifications during oocyte growth correlates with extended parthenogenetic development in the mouse. *Nat. Genet.* **13**, 91-94.

Lee, J. T. (2011). Gracefully ageing at 50, X-chromosome inactivation becomes a paradigm for RNA and chromatin control. *Nat. Rev. Mol. Cell Biol.* **12**, 815-826.

Ma, P., Pan, H., Montgomery, R. L., Olson, E. N. and Schultz, R. M. (2012). Compensatory functions of histone deacetylase 1 (HDAC1) and HDAC2 regulate transcription and apoptosis during mouse oocyte development. *Proc. Natl. Acad. Sci. USA* **109**, E481-E489.

Matsui, T., Leung, D., Miyashita, H., Maksakova, I. A., Miyachi, H., Kimura, H., Tachibana, M., Lorincz, M. C. and Shinkai, Y. (2010). Proviral silencing in embryonic stem cells requires the histone methyltransferase ESET. *Nature* **464**, 927-931.

Nakamura, T., Liu, Y. J., Nakashima, H., Umehara, H., Inoue, K., Matoba, S., Tachibana, M., Ogura, A., Shinkai, Y. and Nakano, T. (2012). PGC7 binds histone H3K9me2 to protect against conversion of 5mC to 5hmC in early embryos. *Nature* **486**, 415-419.

Nesterova, T. B., Barton, S. C., Surani, M. A. and Brockdorff, N. (2001). Loss of Xist imprinting in diploid parthenogenetic preimplantation embryos. *Dev. Biol.* **235**, 343-350.

Peters, A. H. F. M., O'Carroll, D., Scherthan, H., Mechtler, K., Sauer, S., Schöfer, C., Weipoltshammer, K., Pagani, M., Lachner, M., Kohlmaier, A. et al. (2001). Loss of the Suv39h histone methyltransferases impairs mammalian heterochromatin and genome stability. *Cell* **107**, 323-337.

Puschendorf, M., Terranova, R., Boutsma, E., Mao, X., Isono, K.-I., Brykczynska, U., Kolb, C., Otte, A. P., Koseki, H., Orkin, S. H. et al. (2008). PRC1 and Suv39h specify parental asymmetry at constitutive heterochromatin in early mouse embryos. *Nat. Genet.* **40**, 411-420.

Sado, T. and Sakaguchi, T. (2013). Species-specific differences in X chromosome inactivation in mammals. *Reproduction* **146**, R131-R139.

Santos, F., Peters, A. H., Otte, A. P., Reik, W. and Dean, W. (2005). Dynamic chromatin modifications characterise the first cell cycle in mouse embryos. *Dev. Biol.* **280**, 225-236.

Shin, J., Bossenz, M., Chung, Y., Ma, H., Byron, M., Taniguchi-Ishigaki, N., Zhu, X., Jiao, B., Hall, L. L., Green, M. R. et al. (2010). Maternal Rnf12/RLIM is required for imprinted X-chromosome inactivation in mice. *Nature* **467**, 977-981.

Shirane, K., Toh, H., Kobayashi, H., Miura, F., Chiba, H., Ito, T., Kono, T. and Sasaki, H. (2013). Mouse oocyte methylomes at base resolution reveal genome-wide accumulation of non-CpG methylation and role of DNA methyltransferases. *PLoS Genet.* **9**, e1003439.

Sugimoto, M. and Abe, K. (2007). X chromosome reactivation initiates in nascent primordial germ cells in mice. *PLoS Genet.* **3**, e116.

Tada, T. Obata, Y., Tada, M., Goto, Y., Nakatsuji, N., Tan, S., Kono, T. and Takagi, N. (2000). Imprint switching for non-random X-chromosome inactivation during mouse oocyte growth. *Development* **127**, 3101-3105.

Takagi, N. and Sasaki, M. (1975). Preferential inactivation of the paternally derived X chromosome in the extraembryonic membranes of the mouse. *Nature* **256**, 640-642.

Terranova, R., Yokobayashi, S., Stadler, M. B., Otte, A. P., van Lohuizen, M., Orkin, S. H. and Peters, A. H. F. M. (2008). Polycomb group proteins Ezh2 and Rnf2 direct genomic contraction and imprinted repression in early mouse embryos. *Dev. Cell* **15**, 668-679.

Wang, F., Kou, Z., Zhang, Y. and Gao, S. (2007). Dynamic reprogramming of histone acetylation and methylation in the first cell cycle of cloned mouse embryos. *Biol. Reprod.* **77**, 1007-1016.

Wen, B., Wu, H., Shinkai, Y., Irizarry, R. A. and Feinberg, A. P. (2009). Large histone H3 lysine 9 dimethylated chromatin blocks distinguish differentiated from embryonic stem cells. *Nat. Genet.* **41**, 246-250.

Yoshida, N., Brahmajosyula, M., Shoji, S., Amanai, M. and Perry, A. C. (2007). Epigenetic discrimination by mouse metaphase II oocytes mediates asymmetric chromatin remodeling independently of meiotic exit. *Dev. Biol.* **301**, 464-477.